South African Journal of Geomatics, Vol. 10. No. 2, August 2021

A seasonal relationship between land surface temperature and normalized difference bareness index

Subhanil Guha[1] and Himanshu Govil

Department of Applied Geology, National Institute of Technology Raipur, India
[1] subhanilguha@gmail.com

DOI: http://dx.doi.org/10.4314/sajg.v10i2.12

Abstract

The present study analyzes the seasonal variability of the relationship between the land surface temperature (LST) and normalized difference bareness index (NDBaI) on different land use/land cover (LULC) in Raipur City, India by using sixty-five Landsat images of four seasons (pre-monsoon, monsoon, post-monsoon, and winter) of 1991-1992, 1995-1996, 1999-2000, 2004-2005, 2009-2010, 2014-2015, and 2018-2019. The results show that the post-monsoon season indicates the best correlation (0.59), followed by the monsoon (0.56), pre-monsoon (0.47), and winter (0.44) season. The water bodies reflect a strongly positive correlation in all the four seasons (0.65 in pre-monsoon, 0.51 in monsoon, 0.53 in post-monsoon, and 0.62 in winter). On green vegetation, this correlation is also strongly positive in monsoon (0.57), post-monsoon (0.62), and winter (0.55), whereas it is moderate positive in pre-monsoon (0.37) season. The built-up area and bare land build a moderate positive correlation in all the four seasons (0.35 in pre-monsoon, 0.43 in monsoon, 0.48 in post-monsoon, and 0.39 in winter). Among the four seasons, the post-monsoon season builds the best correlation for all LULC types, whereas the pre-monsoon season has the least correlation. This research work is beneficial for land use and environmental planning of any city under similar climatic conditions.

***Keywords**: Landsat; Land surface temperature (LST); Land use/land cover (LULC); Normalized difference bareness index (NDBaI).*

1. Introduction

Land surface temperature (LST) is a significant factor in analyzing the bio-geochemical functions of the land surface features (Tomlinson et al. 2011; Hao et al. 2016; Guha 2017). Green plants, wetlands, and water bodies generate low LST, whereas human settlement, and bare land surface produce high LST in the summer season of tropical areas (Chen et al. 2006; Guha et al. 2020). Thus, LST related studies are quite important in the ecological planning of the recent urban agglomerations (Li et al. 2016). Normalized difference bareness index (NDBaI) is the most popular index for bare land extraction that is invariably used in LULC and LST related studies (Zhao and Chen 2005; Chen

et al. 2006; Weng and Quattrochi 2006; Essa et al. 2012; Chen et al. 2013; Guha et al. 2019; Yuan et al. 2017).

Several research articles presented the LST-NDBaI relationship in different parts of the world. As-Syakur et al. (2012) investigates various bareness indices for bare land mapping in Denpasar of Bali, Indonesia. Ahmed (2013) used NDBaI along with other LULC indices to simulate the land surface changes and their impact on LST in Dhaka, Bangladesh. Sharma et al. (2013) examined the relationship between LST and NDBaI in Surat City of India. Guo et al. (2014) estimated sub-pixel LST and built a relationship between LST and NDBaI in Guangzhou core urban area of China. Ali et al. (2017) compared the relationship of LST with NDBaI and other LULC indices in London and Baghdad cities. Macarof et al. (2017) investigated the relationship between LST and NDBaI in Iaşi Municipality Area of eastern Romania from 2013 to 2016 by using Landsat 8 data. Alibakshi et al. (2019) investigated the relationship between NDBaI and LST from 2001 to 2015 in Tehran and its satellite cities in Iran by the geographically weighted regression model using Landsat 7 data. Alexander (2020) evaluated the LST-NDBaI relationship in Aarhus City of Denmark by using Landsat 8 data. Jain et al. (2020) investigated the LST-NDBaI relationship in Nagpur City, India from 2000 to 2015 by using Landsat data.

The nature of LST and NDBaI changes due to the seasonal changes of various atmospheric components. Thus, to reveal the characteristics of seasonal variation of the LST-NDBaI relationship in a tropical city, we have selected the Raipur City of Chhattisgarh State in India. The main aim of the study is to determine the seasonal variation of LST-NDBaI relationship on different LULC types. The study will be a beneficial one ecological planning and management. The seasonal LST-NDBaI relationship means the relationship between LST and NDBaI in different seasons like pre-monsoon, monsoon, post-monsoon, and winter. It is determined by using a number of Landsat satellite data of these four aforesaid seasons from 1991-92 to 2018-19. The study tries to establish a long-term relationship between LST and NDBaI for various seasons and also on different types land use/land cover. No such type of study has been conducted on this city before the work. The study is beneficial for ecological planning because it focuses on the LST-NDBaI relationship on different LULC types.

2. Study area and data

Figure 1 shows the geographical location of Raipur city of India which extends from 21°11'22"N to 21°20'02"N and from 81°32'20"E to 81°41'50"E. The city covers an area of around 165 km^2. The upper left corner of the figure presents the outline map of India where Chhattisgarh State is located in the middle part (http://www.surveyofindia.gov.in). The lower left corner of the figure presents the outline map of Chhattisgarh State with districts (http://www.surveyofindia.gov.in). The upper right corner of the figure represents the false colour composite (FCC) image of Raipur city (https://raipur.gov.in) from recent Landsat 8 OLI/TIRS data of 22 October 2018 (https://www.earthexplorer.usgs.gov). The lower right corner of the figure indicates the digital

elevation map (DEM) of Raipur city produced by the ArcGIS software using the last available ASTER DEM data of 11 October 2011 (https://www.earthexplorer.usgs.gov). The city is characterised by the tropical dry and wet type of climate (http://www.imdraipur.gov.in). The mean monthly temperature ranges from 12ºC to 42ºC. May presents the highest average temperature (35ºC), while December presents the lowest average temperature (20ºC). The highest average rainfall (327 mm) is observed in July. March, April, and May are considered as the summer or pre-monsoon months.

Table 1 shows the Landsat data sets used in this study. LST was retrieved through the TIR bands of Landsat data sets [band 6 for Landsat 5 Thematic Mapper (TM) and Landsat 7 Enhanced Thematic Mapper Plus (ETM+) data, whereas band 10 for Landsat 8 Operational Land Imager (OLI)/ Thermal Infrared Sensors (TIRS) data]. The whole study was performed by using ArcGIS 9.3 software. Landsat 8 TIRS dataset has two TIR bands (bands 10 and 11) in which band 11 has a larger calibration uncertainty. Thus, only TIR band 10 data (100 m resolution) has been recommended for the present study (Barsi et al. 2014). The TIR band of Landsat 5 TM data and Landsat 7 ETM+ data is band 6. The TIR bands of each Landsat sensors have been resampled to 30 m x 30 m pixel size by the data provider (EROS) using the cubic convolution resampling method.

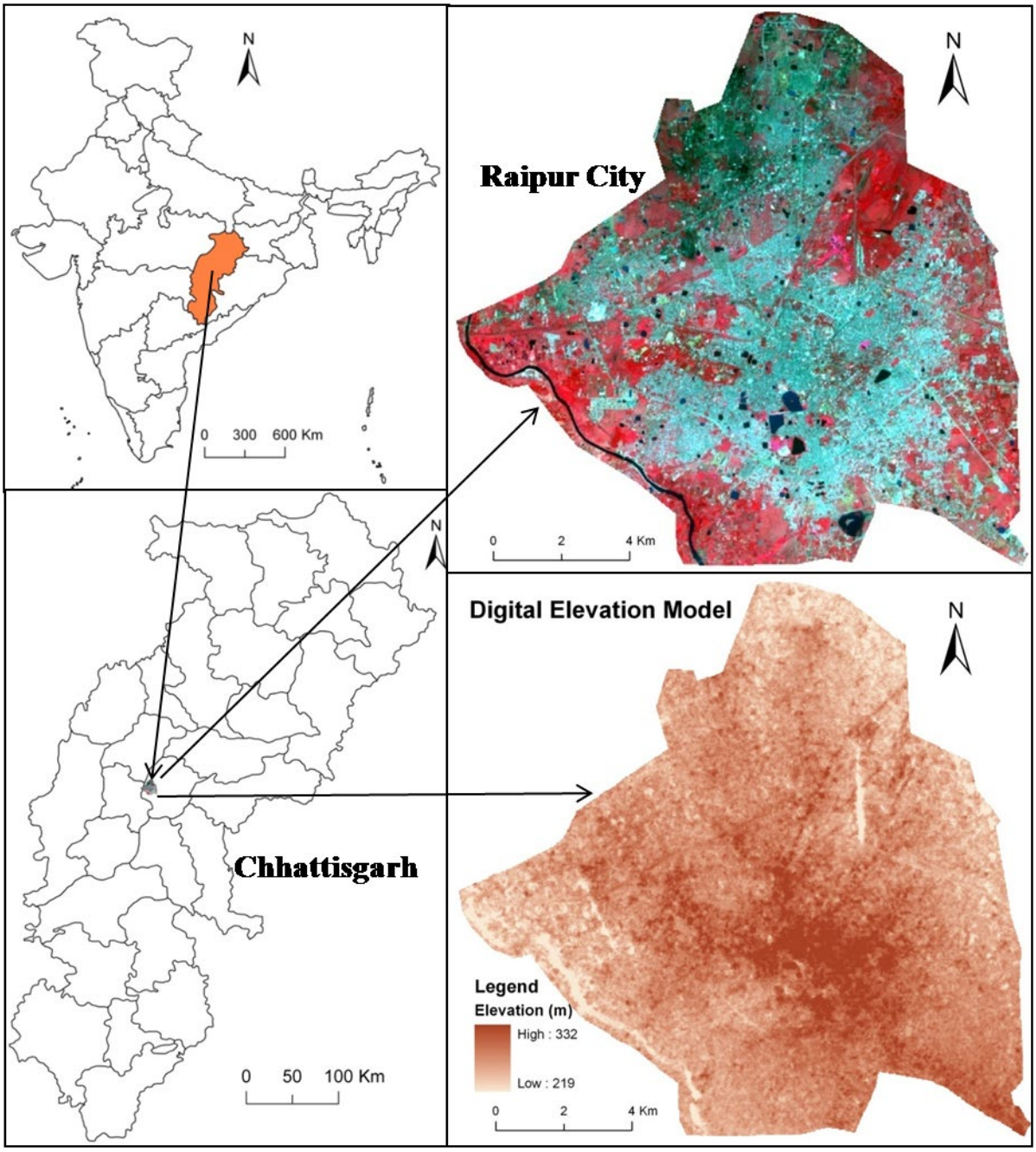

Figure 1. Location of the study area.

Table 1: Specification of Landsat data sets.

Landsat scene ID	Date of acquisition	Time (UTC)	Sun elevation (°)	Sun azimuth (°)	Cloud cover (%)	Earth-Sun distance (astronomical unit)	Resolution of TIR bands (m)
LT51420451991077ISP00	18-Mar-91	04:17:34	48.58	118.92	0	0.99	120
LT51420451991093ISP00	03-Apr-91	04:17:46	53.04	111.64	0	0.99	120
LT51420451991141ISP00	21-May-91	04:18:39	59.93	87.09	1	1.01	120
LT51420451991269ISP01	26-Sep-91	04:20:03	52.47	123.30	13	1.00	120
LT51420451991285BKT02	12-Oct-91	04:20:12	42.22	131.85	6	0.99	120
LT51420451991317ISP00	13-Nov-91	04:20:19	41.53	142.35	1	0.99	120
LT51420451992016ISP00	16-Jan-92	04:20:22	35.26	139.03	3	0.98	120
LT51420451992032BKT01	01-Feb-92	04:20:27	37.41	135.03	0	0.98	120
LT51420451992048ISP00	17-Feb-92	04:20:15	40.89	130.26	4	0.98	120
LT51420451995104ISP01	14-Apr-95	04:05:06	52.75	103.75	0	1.00	120
LT51420451995344BKT00	10-Dec-95	03:56:47	33.01	139.15	0	0.98	120
LT51420451996027ISP00	27-Jan-96	04:00:14	33.31	132.27	0	0.98	120
LT51420451996267ISP00	23-Sep-96	04:14:16	51.81	120.64	2	1.00	120
LT51420451996283ISP00	09-Oct-96	04:15:07	48.92	129.53	0	0.99	120
LT51420451996299ISP00	25-Oct-96	04:15:55	45.37	136.48	5	0.99	120
LT51420451996315ISP00	10-Nov-96	04:16:41	41.61	141.11	7	0.99	120
LE71420451999315SGS00	11-Nov-99	04:49:00	45.72	149.96	0	0.99	60
LE71420452000030SGS00	30-Jan-00	04:48:55	41.46	142.31	0	0.98	60
LE71420452000094SGS00	03-Apr-00	04:48:35	59.72	118.62	0	1.00	60
LE71420452000126SGS00	05-May-00	04:48:20	65.97	98.50	0	1.00	60
LE71420452000270SGS00	26-Sep-00	04:46:33	57.21	131.59	6	1.00	60
LE71420452000350SGS00	15-Dec-00	04:46:31	38.94	150.22	0	0.98	60
LT51420452004081BKT00	21-Mar-04	04:35:14	53.26	121.40	0	0.99	120
LT51420452004113BKT00	22-Apr-04	04:36:01	61.43	104.47	1	1.00	120
LT51420452004145BKT00	24-May-04	04:36:54	64.25	86.72	0	1.00	120
LT51420452004161BKT00	09-Jun-04	04:37:23	63.98	81.78	9	1.01	120
LT51420452004273BKT00	29-Sep-04	04:40:16	55.47	131.40	9	1.00	120
LT51420452004289BKT00	15-Oct-04	04:40:36	51.63	139.65	4	0.99	120
LT51420452004321BKT00	16-Nov-04	04:41:11	43.41	148.58	0	0.98	120
LT51420452004337BKT00	02-Dec-04	04:41:33	40.14	149.58	0	0.98	120
LT51420452004353BKT00	18-Dec-04	04:41:52	38.12	148.74	0	0.98	120
LT51420452005019BKT00	19-Jan-05	04:42:17	38.92	143.21	0	0.98	120
LT51420452005035BKT00	04-Feb-05	04:42:29	41.74	139.16	0	0.98	120
LT51420452009062KHC01	03-Mar-09	04:42:22	49.04	130.64	0	0.99	120
LT51420452009078KHC00	19-Mar-09	04:42:44	54.10	124.40	2	0.99	120
LT51420452009094BKT00	04-Apr-09	04:43:05	58.86	116.70	0	1.00	120
LT51420452009110BKT00	20-Apr-09	04:43:24	62.67	107.39	0	1.00	120
LT51420452009126BKT00	06-May-09	04:43:42	65.03	97.25	0	1.00	120
LT51420452009142KHC00	22-May-09	04:44:00	65.88	88.22	1	1.00	120
LT51420452009174KHC00	23-Jun-09	04:44:35	64.96	80.76	0	1.00	120
LT51420452009286KHC00	13-Oct-09	04:46:12	53.04	140.48	0	0.99	120
LT51420452009302BKT00	29-Oct-09	04:46:20	48.72	146.41	0	0.99	120
LT51420452009350KHC00	16-Dec-09	04:46:44	38.90	150.21	1	0.99	120
LT51420452010017KHC00	17-Jan-10	04:46:55	39.27	144.86	6	0.99	120
LT51420452010033KHC00	02-Feb-10	04:46:59	41.92	140.89	0	0.98	120
LT51420452010049KHC00	18-Feb-10	04:47:02	45.89	136.27	7	0.98	100
LC81420452014076LGN01	17-Mar-14	04:56:36	55.95	129.38	0	0.99	100
LC81420452014092LGN01	02-Apr-14	04:56:19	60.91	121.72	0	0.99	100
LC81420452014140LGN01	20-May-14	04:55:38	68.56	90.40	5	1.01	100
LC81420452014156LGN01	05-Jun-14	04:55:45	68.38	83.30	0	1.01	100
LC81420452014316LGN01	12-Nov-14	04:56:21	46.22	152.46	7	0.98	100
LC81420452014364LGN01	30-Dec-14	04:56:09	39.34	150.83	0	0.98	100
LC81420452015015LGN01	15-Jan-15	04:56:09	40.22	147.71	0	0.98	100
LC81420452015031LGN01	31-Jan-15	04:56:04	42.76	143.86	0	0.98	100
LC81420452015047LGN01	16-Feb-15	04:55:55	46.67	139.41	0	0.98	100
LC81420452018071LGN00	12-Mar-18	04:55:43	54.19	131.16	2	0.99	100
LC81420452018087LGN00	28-Mar-18	04:55:36	59.29	124.07	0	0.99	100
LC81420452018135LGN00	15-May-18	04:55:08	68.27	93.32	0	1.01	100
LC81420452018167LGN00	16-Jun-18	04:55:01	67.74	81.10	2	1.01	100
LC81420452018279LGN00	06-Oct-18	04:55:53	56.39	140.40	0	0.99	100
LC81420452018295LGN00	22-Oct-18	04:55:59	51.96	147.33	0	0.99	100
LC81420452018311LGN00	07-Nov-18	04:56:03	47.49	151.56	0	0.99	100
LC81420452018359LGN00	25-Dec-18	04:55:59	39.40	151.57	0	0.98	100
LC81420452019042LGN00	11-Feb-19	04:55:52	45.33	140.84	0	0.98	100
LC81420452019058LGN00	27-Feb-19	04:55:48	49.94	135.93	4	0.99	100

3. Methodology

3.1. Retrieving LST from Landsat data

In this study, the mono-window algorithm was applied to retrieve LST from multi-temporal Landsat satellite sensors where three necessary parameters are ground emissivity, atmospheric transmittance, and effective mean atmospheric temperature (Qin et al. 2001; Weng et al. 2004; Wang et al. 2016; Sekertekin and Bonafoni 2020). At first, the original TIR bands (100 m resolution for Landsat 8 OLI/TIRS data, 120 m resolution for Landsat 5 TM data and Landsat 7 ETM+ data) were resampled into 30 m by USGS data centre for further application.

The TIR pixel values are firstly converted into radiance from digital number (DN) values. Radiance for TIR band of Landsat 5 TM data and Landsat 7 ETM+ data is obtained using equation [1] (USGS):

$$L_\lambda = \left[\frac{L_{MAX\lambda} - L_{MIN\lambda}}{QCAL_{MAX} - QCAL_{MIN}}\right] * [Q_{CAL} - QCAL_{MIN}] + L_{MIN\lambda} \quad [1]$$

where, L_λ is Top of Atmosphere (TOA) spectral radiance ($Wm^{-2}sr^{-1}mm^{-1}$), Q_{CAL} is the quantized calibrated pixel value in DN, $L_{MIN\lambda}$ ($Wm^{-2}sr^{-1}mm^{-1}$) is the spectral radiance scaled to $QCAL_{MIN}$, $L_{MAX\lambda}$ ($Wm^{-2}sr^{-1}mm^{-1}$) is the spectral radiance scaled to $QCAL_{MAX}$, $QCAL_{MIN}$ is the minimum quantized calibrated pixel value in DN and $QCAL_{MAX}$ is the maximum quantized calibrated pixel value in DN. $L_{MIN\lambda}$, $L_{MAX\lambda}$, $QCAL_{MIN}$, and $QCAL_{MAX}$values are obtained from the metadata file of Landsat TM and ETM+ data. Radiance for Landsat 8 TIR band is obtained from equation [2] (Zanter 2019):

$$L_\lambda = M_L . Q_{CAL} + A_L \quad [2]$$

where, L_λ is the TOA spectral radiance ($Wm^{-2}sr^{-1}mm^{-1}$), M_L is the band-specific multiplicative rescaling factor from the metadata, A_L is the band-specific additive rescaling factor from the metadata, $Q_{CAL}$is the quantized and calibrated standard product pixel values (DN). All of these variables can be retrieved from the metadata file of Landsat 8 data.

For Landsat 5 data, the reflectance value is obtained from radiances using equation [3] (USGS):

$$\rho_\lambda = \frac{\pi . L_\lambda . d^2}{ESUN_\lambda . cos\,\theta_s} \quad [3]$$

where, $\rho_\lambda$is unitless planetary reflectance, L_λ is the TOA spectral radiance ($Wm^{-2}sr^{-1}\mu m^{-1}$), $d$is Earth-Sun distance in astronomical units, $ESUN_\lambda$ is the mean solar exo-atmospheric spectral irradiances ($Wm^{-2}\mu m^{-1}$) and θ_s is the solar zenith angle in degrees. $ESUN_\lambda$ values for each band of Landsat 5 and 7 data can be obtained from the handbooks of the related mission. θ_s and $d$values can be attained from the metadata file.

For Landsat 8 data, reflectance conversion can be applied to DN values directly as in equation [4] (Zanter 2019):

$$\rho_\lambda = \frac{M_\rho \cdot Q_{CAL} + A_\rho}{\sin \theta_{SE}} \quad [4]$$

where, M_ρ is the band-specific multiplicative rescaling factor from the metadata, $A_\rho$is the band-specific additive rescaling factor from the metadata, Q_{CAL} is the quantized and calibrated standard product pixel values (DN) and $\theta_{SE}$is the local sun elevation angle from the metadata file.

Equation [5] is used to convert the spectral radiance to at-sensor brightness temperature (Wukelic et al. 1989; Chen et al. 2006):

$$T_b = \frac{K_2}{ln(\frac{K_1}{L_\lambda}+1)} \quad [5]$$

where, $T_b$is the brightness temperature in Kelvin (K), L_λ is the spectral radiance in $Wm^{-2}sr^{-1}mm^{-1}$; $K_2$and $K_1$are calibration constants. For Landsat 8 data, K_1 is 774.89, K_2 is 1321.08 ($Wm^{-2}sr^{-1}mm^{-1}$). For Landsat 7 data, is 666.09, is 1282.71 ($Wm^{-2}sr^{-1}mm^{-1}$). For Landsat 5 data, K_1 is 607.76, K_2 is 1260.56 ($Wm^{-2}sr^{-1}mm^{-1}$). K_1 K_2

The land surface emissivityε, is estimated from equation [6] using the NDVI Thresholds Method (Sobrino et al. 2001; 2004).

$$\varepsilon = \varepsilon_v F_v + \varepsilon_s(1 - F_v) + d\varepsilon \quad [6]$$

where, ε is land surface emissivity, ε_v is vegetation emissivity, $\varepsilon_s$is soil emissivity, $Fv$is fractional vegetation, $d\varepsilon$is the effect of the geometrical distribution of the natural surfaces and internal reflections that can be expressed by equation [7]:

$$d\varepsilon = (1 - \varepsilon_s)(1 - F_v)F\varepsilon_v \quad [7]$$

where, ε_v is vegetation emissivity, $\varepsilon_s$is soil emissivity, $Fv$is fractional vegetation, $F$is a shape factor whose mean is 0.55, the value of $d\varepsilon$may be 2% for mixed land surfaces (Sobrino et al. 2004).

The fractional vegetationF_v, of each pixel, is determined from the NDVI using equation [8] (Carlson and Repley 1997):

$$F_v = \left(\frac{NDVI - NDVI_{min}}{NDVI_{max} - NDVI_{min}} \right)^2 \quad [8]$$

where, $(a) NDVI < 0.2$ for bare soil; $(b) NDVI > 0.5$ for vegetation; $(c) 0.2 <= NDVI <= 0.5$ for mixed land with bare soil and vegetation (Sobrino et al. 2001; 2004).

Finally, the land surface emissivity ε can be expressed by equation [9]:

$$\varepsilon = 0.004 * F_v + 0.986 \quad [9]$$

where, ε is land surface emissivity, $Fv$is fractional vegetation.

Water vapour content is estimated by equation [10] (Yang and Que 1996; Li 2006):

$$w = 0.0981 * \left[10 * 0.6108 * exp\left(\frac{17.27*(T_0-273.15)}{237.3+(T_0-273.15)}\right) * RH\right] + 0.1697 \quad [10]$$

where, $w$is the water vapour content (g/cm^2), $T_0$is the near-surface air temperature in Kelvin (K), RH is the relative humidity (%). These parameters of atmospheric profile are obtained from the Meteorological Centre, Raipur (http://www.imdraipur.gov.in). Atmospheric transmittance is determined for Raipur City using equation [11] (Qin 2001; Sun 2010):

$$\tau = 1.031412 - 0.11536w \quad [11]$$

where, $\tau$is the total atmospheric transmittance, $w$is the water vapour content (g/cm^2).

Raipur City is located in the tropical region. Thus, equation [12] is applied to compute the effective mean atmospheric transmittance of Raipur (Qin 2001; Sun 2010):

$$T_a = 17.9769 + 0.91715T_0 \quad [12]$$

LST is retrieved from Landsat 5 TM and Landsat 8 OLI/TIRS satellite data by using equations [13-15] (Qin 2001):

$$T_s = \frac{[a(1-C-D)+(b(1-C-D)+C+D)T_b-DT_a]}{C} \quad [12]$$

$$C = \varepsilon\tau \quad [13]$$

$$D = (1-\tau)[1+(1-\varepsilon)\tau] \quad [14]$$

where, $\varepsilon$is the land surface emissivity, $\tau$is the total atmospheric transmittance, C and D are internal parameters based on atmospheric transmittance and land surface emissivity, $T_b$is the at-sensor brightness temperature, $T_a$is the mean atmospheric temperature, $T_0$is the near-surface air temperature, $T_s$is the land surface temperature, $a = -67.355351$, $b = 0.458606$.

3.2. Extraction of different types of LULC by using NDBaI

In this study, special emphasis has been given on NDBaI for determining the relationship with LST (Chen et al. 2006; Zhao and Chen 2005). NDBaI is determined by the short wave infrared (SWIR) and thermal infrared (TIR) bands. For, Landsat 5 TM and Landsat 7 ETM+ data, band 5 is used as the SWIR band and band 6 is used as TIR band, respectively. For Landsat 8 OLI and TIRS data, band 6 and band 10 are used as the TIR bands, respectively (Table 2). The value of NDBaI is ranged between −1 and +1. Generally, the positive value of NDBaI indicates the bare land (Table 2). The bareness increases with the increase of the positive NDBaI. NDBaI value ranges between -0.2 to 0 shows the built-up area, whereas NDBaI > 0 shows the bare land [3]. NDBaI is also used to extract other LULC types, e.g., vegetation (NDBaI < -0.25), and water bodies (NDBaI < -0.65). LULC maps have been generated using the aforesaid threshold limits of NDBaI and the results have been validated

by the maximum likelihood classification. The average calculated values of the Kappa coefficient and overall accuracy for all the images are 0.91 and 92.19%, respectively.

Table 2. Description of NDBaI and its threshold values used for extracting the various types of LULC.

Acronym	Description	Formulation	References	Threshold limits of NDBaI for extracting different LULC types			
				Vegetation	Water bodies	Built-up area	Bare land
NDBaI	Normalized difference bareness index		Zhao and Chen 2005; Chen et al. 2006	< -0.25	< -0.65	-0.2 - 0	> 0

4. Results and discussion

4.1. Extraction of LULC types using NDBaI

Figure 2 shows the LULC maps of the post-monsoon Landsat images of different years. LULC maps have been generated using the threshold limits of NDBaI. In 1991-92, the built-up area and bare land were mainly found in the central part of the Raipur City. The northwest portion of the city has been urbanized rapidly from 1991-92 to 2004-05 as the percentage of urban vegetation has been declined due to the conversion into built-up areas. After 2004-05, the green areas have been reduced at an alarming rate as most of the parts of the city have been converted into bare land and built-up area. Only the east and the southwest parts were covered by urban vegetation. Water bodies are the most stable LULC type in the study area. Green vegetation has been decreased in a very significant amount (76.80 km^2) from 1991-92 to 2018-19. On the other hand, the built-up area and bare land have been increased at a very high rate (78.37 km^2 in 27 years) due to rapid land conversion.

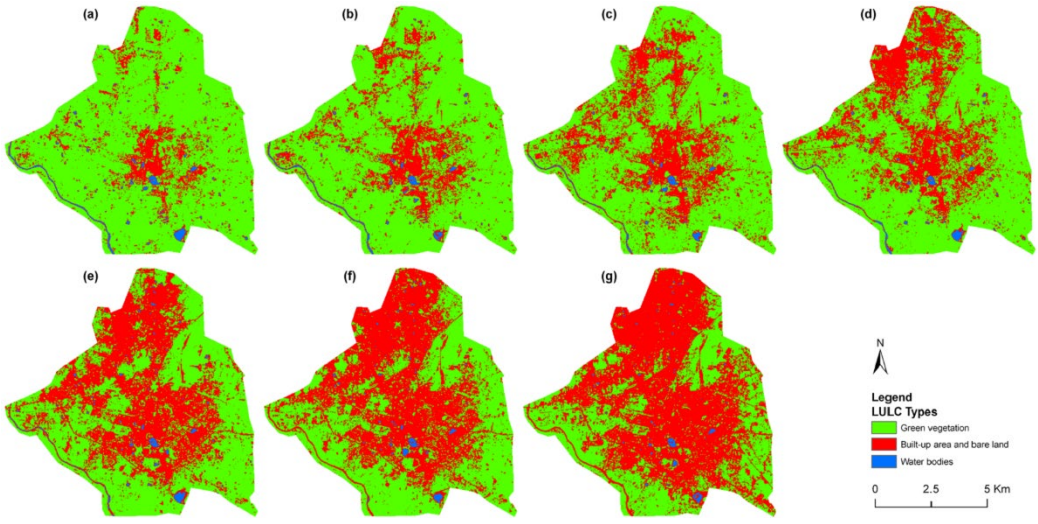

Figure 2. LULC maps of the study area for the following years: (a) 1991-92 (b) 1995-96 (c) 1999-00 (d) 2004-05 (e) 2009-10 (f) 2014-15 (g) 2018-19.

4.2. Characteristics of the spatial distribution of LST and NDBaI

There is a prominent seasonal variation of different periods that occurred in mean and standard deviation (STD) values of LST (Table 3). The winter season indicates the lowest mean LST values for all the years, whereas the highest mean LST values are found in the pre-monsoon seasons during the entire span. From 1991-92 to 2018-19, the mean LST has increased in every season. The post-monsoon season has the mean LST value nearer to the winter season, while monsoon season has a slightly high value of mean LST than the post-monsoon season. The average values of LST and the correlation coefficient of LST and NDBaI from 1991-92 to 2018-19 have been shown in grey shades inside Table 3.

Table 3. Temporal and seasonal variation of LST values and Pearson's correlation coefficient values of LST-NDBaI relationship (significant al 0.05 level).

Season	Year of acquisition	LST (°C)				Correlation coefficients for LST-NDBaI relationship
		Min.	Max.	Mean	Std.	
Pre-monsoon	1991-92	23.81	36.27	31.54	1.52	0.58
	1995-96	24.54	41.07	34.64	1.89	0.51
	1999-00	26.36	42.23	36.38	1.93	0.49
	2004-05	26.95	44.07	38.01	2.19	0.48
	2009-10	28.81	46.48	39.60	2.54	0.43
	2014-15	31.93	48.22	41.28	1.75	0.41
	2018-19	33.46	51.11	43.74	1.75	0.40
	Average	27.98	44.21	37.88	1.94	0.47
Monsoon	1991-92	19.87	30.83	25.74	1.41	0.66
	1995-96	21.21	33.01	26.50	1.33	0.54
	1999-00	22.76	35.91	27.81	1.34	0.53
	2004-05	24.17	36.20	31.32	1.33	0.54
	2009-10	25.94	38.38	33.06	2.40	0.56
	2014-15	27.74	40.15	34.87	1.68	0.50
	2018-19	30.59	41.98	37.30	1.13	0.55
	Average	24.61	36.64	30.94	1.52	0.56
Post-monsoon	1991-92	19.72	29.56	24.32	1.72	0.69
	1995-96	20.42	30.33	25.12	1.34	0.59
	1999-00	22.41	33.47	26.84	1.91	0.57
	2004-05	23.03	35.25	28.01	1.71	0.56
	2009-10	24.62	37.91	30.26	1.60	0.58
	2014-15	26.24	38.22	31.68	1.12	0.56
	2018-19	28.92	41.28	33.70	1.34	0.57
	Average	23.62	35.15	28.56	1.53	0.59
Winter	1991-92	18.22	28.33	23.29	1.22	0.53
	1995-96	20.08	28.68	24.40	1.04	0.48
	1999-00	20.44	32.80	25.21	1.81	0.46
	2004-05	21.08	33.21	26.47	1.25	0.44
	2009-10	22.06	34.36	27.98	1.23	0.42
	2014-15	22.80	36.21	28.90	1.39	0.41
	2018-19	24.31	38.36	30.46	1.37	0.37
	Average	21.28	33.14	26.67	1.33	0.44

The pre-monsoon season has the maximum values of mean LST (31.54°C in 1991-92, 34.64°C in 1995-96, 36.38°C in 1999-00, 38.01°C in 2004-05, 39.60°C in 2009-10, 41.28°C in 2014-15, and 43.74°C in 2018-19) (Figure 3), followed by monsoon (Figure 4), post-monsoon (Figure 5), and

winter (Figure 6) season. At the macro-level, the areas with high LST values show the urban heat island phenomenon. These areas have relatively high NDBaI values. At the micro-level, the high peaks of LST also presented the high peaks of NDBaI. The correlation coefficient values of Pearson's linear correlation between the LST and NDBaI are positive (for any year or season). The post-monsoon season has the best mean (mean value of 1991-92, 1995-96, 1999-00, 2004-05, 2009-10, 2014-15, and 2018-19) correlation coefficient value (0.59), followed by the monsoon (0.56), pre-monsoon (0.48), and winter (0.44) season. It is seen from Figure 3 that in 2018-19, more than 90% of the area in the pre-monsoon season was above 40°C LST. The picture is different in the winter season, where no area of the city was above 40°C LST. In 1991-92, almost 90% of the area was below 25°C LST in the winter season (Figure 6). The monsoon (Figure 4) and post-monsoon (Figure 5) seasons indicate a moderate range of LST. The mean LST of the study area has been gradually increased between 1991-92 and 2018-19. The conversion of other lands into the built-up area and bare land influences a lot on the mean LST of the city. Both the changed and unchanged built-up area and bare land suffer from the increasing trend of LST. These results significantly present the influence of climate change in Raipur City.

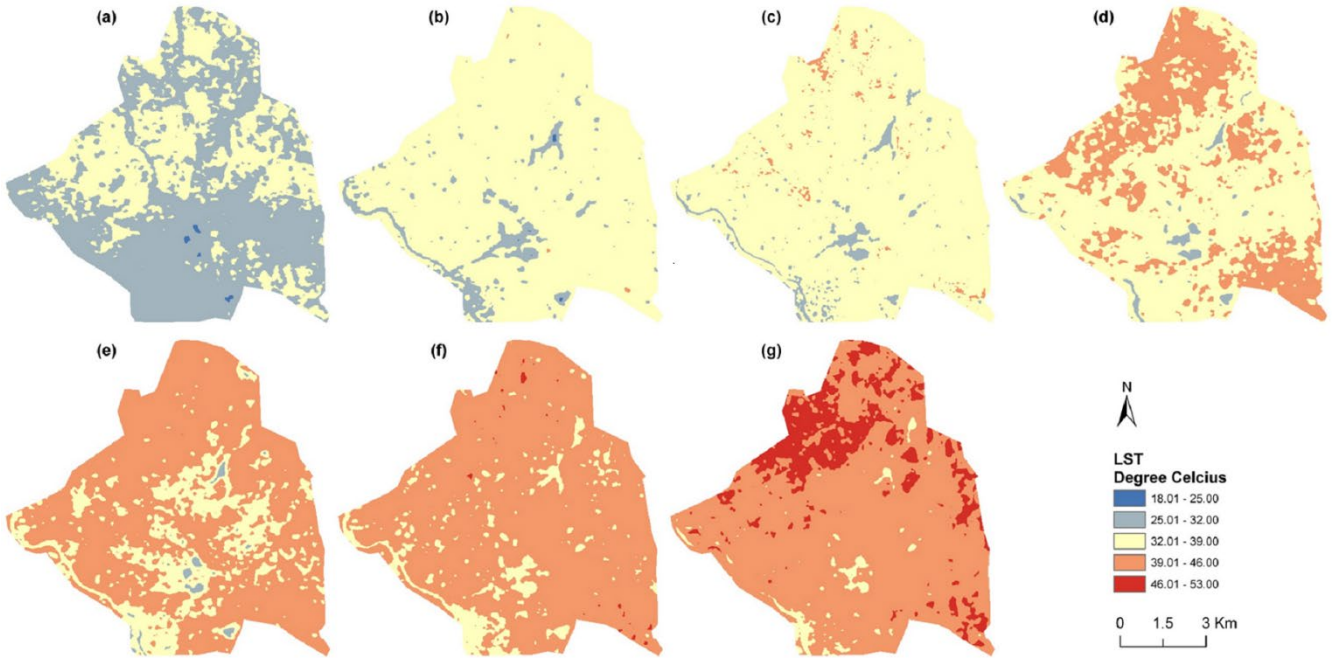

Figure 3. Spatial distribution of LST in pre-monsoon season for the following years: (a) 1991-92 (b) 1995-96 (c) 1999-00 (d) 2004-05 (e) 2009-10 (f) 2014-15 (g) 2018-19 2004-05 (e1-e4) 2009-10 (f1-f4) 2014-15 (g1-g4) 2018-19.

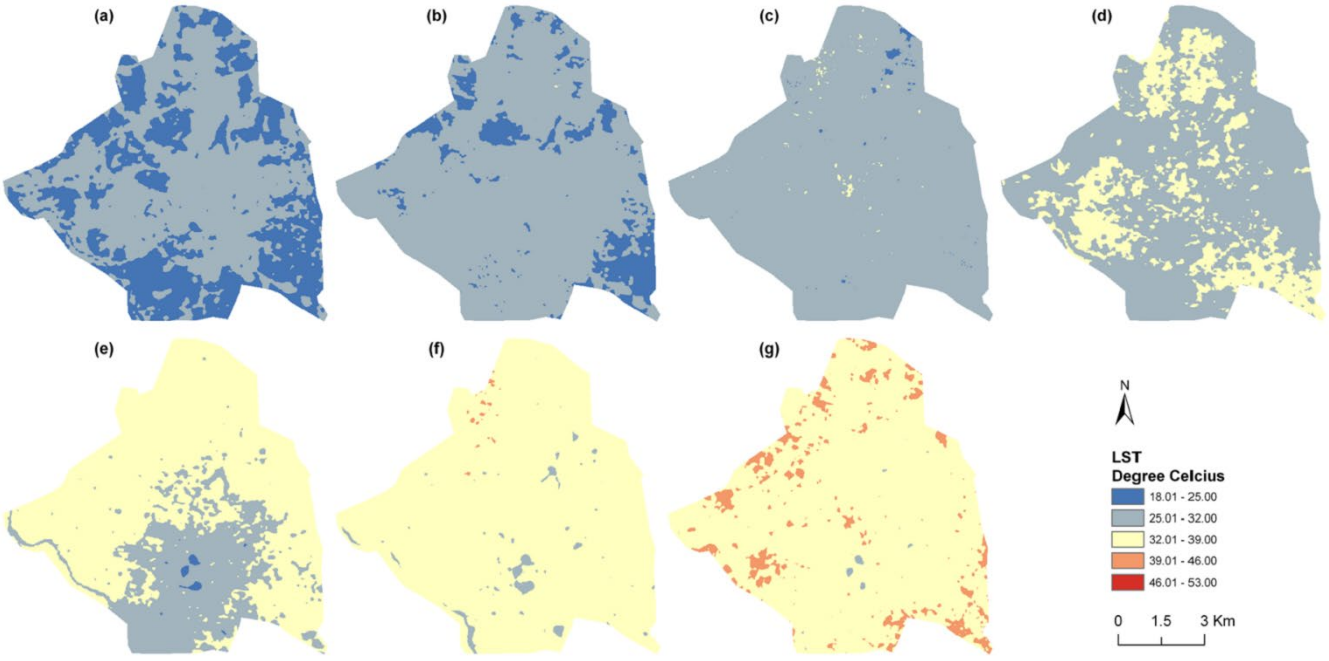

Figure 4. Spatial distribution of LST in monsoon season for the following years: (a) 1991-92 (b) 1995-96 (c) 1999-00 (d) 2004-05 (e) 2009-10 (f) 2014-15 (g) 2018-19 2004-05 (e1-e4) 2009-10 (f1-f4) 2014-15 (g1-g4) 2018-19.

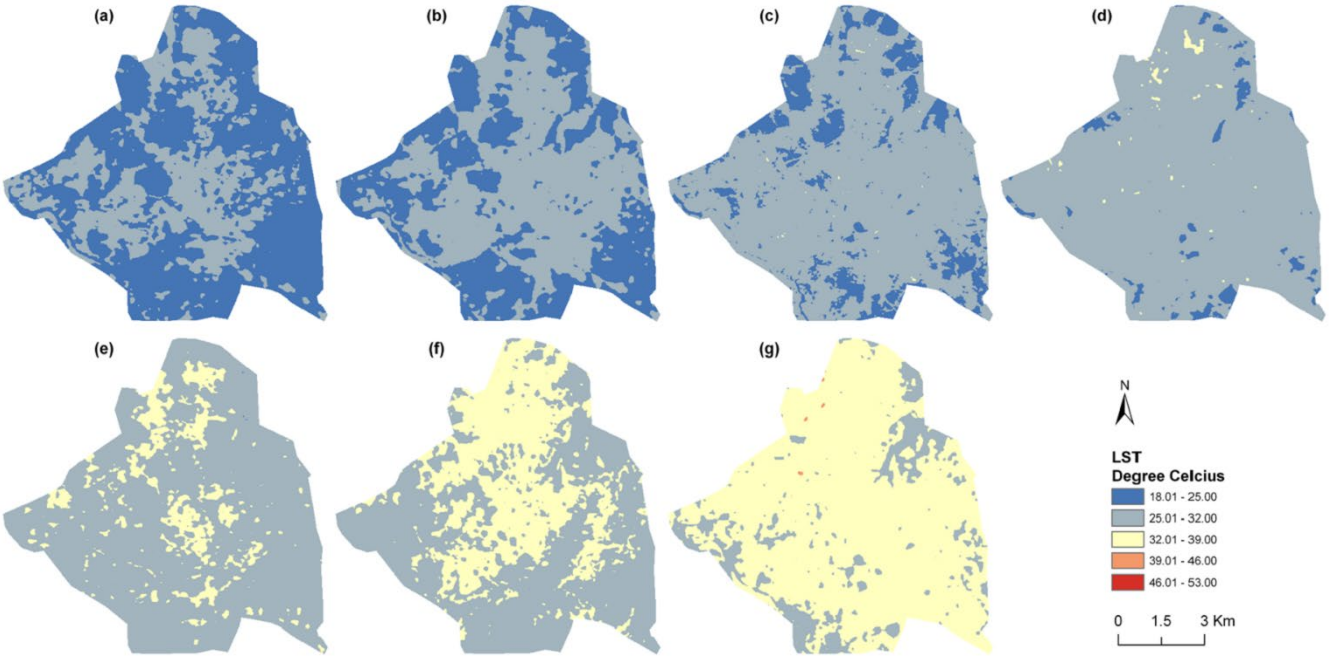

Figure 5. Spatial distribution of LST in post-monsoon season for the following years: (a) 1991-92 (b) 1995-96 (c) 1999-00 (d) 2004-05 (e) 2009-10 (f) 2014-15 (g) 2018-19 2004-05 (e1-e4) 2009-10 (f1-f4) 2014-15 (g1-g4) 2018-19.

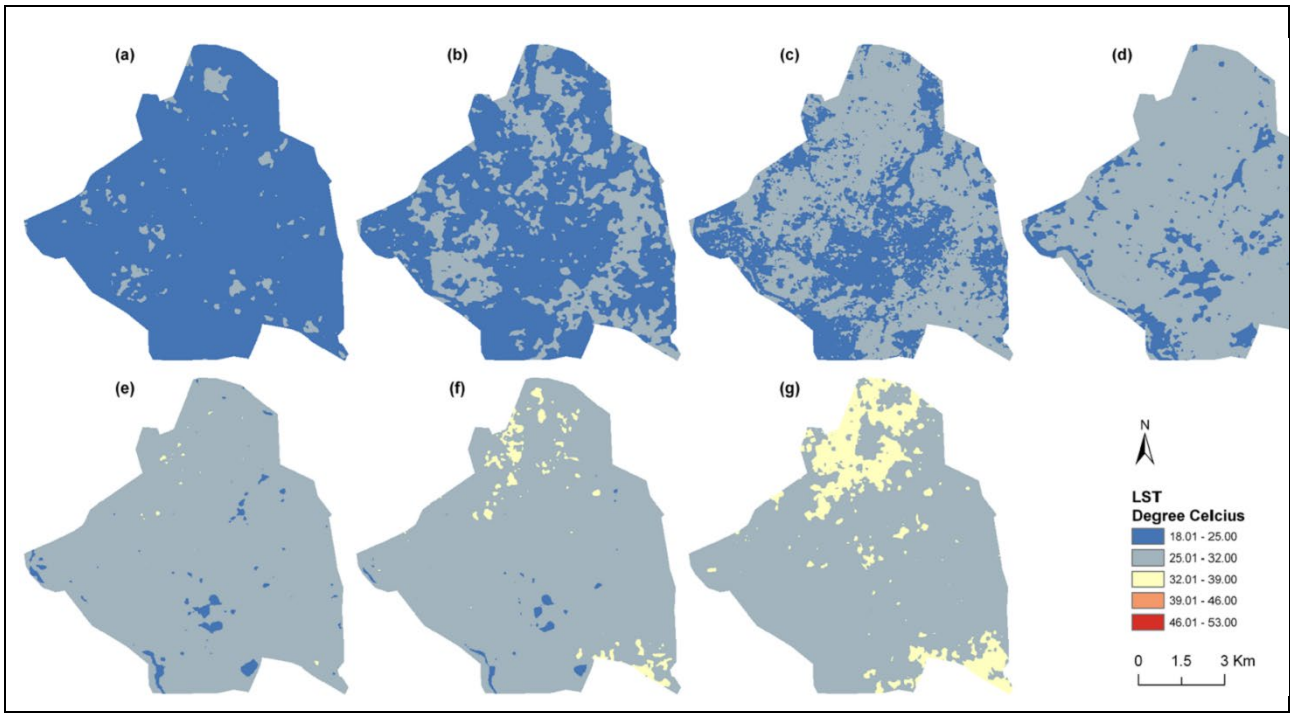

Figure 6. Spatial distribution of LST in winter season for the following years: (a) 1991-92 (b) 1995-96 (c) 1999-00 (d) 2004-05 (e) 2009-10 (f) 2014-15 (g) 2018-19 2004-05 (e1-e4) 2009-10 (f1-f4) 2014-15 (g1-g4) 2018-19.

4.3. Seasonal variation on LST-NDBaI relationship

Figure 7 (a-d) shows the seasonal variation of LST-NDBaI relationships on different LULC types in winter, pre-monsoon, monsoon, and post-monsoon season, respectively. Here, only three types of LULC are considered, i.e., (1) vegetation, (2) water bodies, and (3) built-up area and bare land. On water bodies, the LST-NDBaI relationship is strongly positive for any season. NDBaI is a bareness index that is frequently used in bare land extraction. On the bare land and built-up area of the study area, the correlation is a moderate positive for all four seasons. On green vegetation, the relationship is strong (monsoon, post-monsoon, and winter) to moderate (pre-monsoon) positive. The pre-monsoon season (Figure 7 (a)) has a strong positive LST-NDBaI correlation on the water bodies (0.65) and a moderate positive correlation on green vegetation (0.37), bare land, and built-up area (0.35). In the monsoon season, the correlation is strongly positive on green vegetation (0.56) and water bodies (0.51), whereas the correlation is moderate positive (0.43) on bare land and built-up area (Figure 7 (b)). The post-monsoon season has a stable and strong positive correlation (correlation coefficient > 0.48) for any LULC categories throughout the period (Figure 7 (c)). The best correlation has been built on green vegetation (0.62), followed by the water bodies (0.53), bare land and built-up area (0.48). In winter (Figure 7 (d)), the LST-NDBaI correlation is strongly positive on water bodies (0.62) and green vegetation (0.54). Bare lands and built-up areas reflect the moderate positive (0.39) correlation in the winter season because at that time dry soil, exposed rock surface, and building materials get cooler than green vegetation and water bodies. Figure 7 (e) represents a generalized

view of the overall seasonal variation of LST-NDBaI relationships for the whole of the study area. The relationship is positive, irrespective of any season. It can be concluded from Figure 7 (e) that the post-monsoon season reveals the best correlation among all the four seasons. It is mainly because of the high intensity of moisture content in the air. Dry seasons (winter and pre-monsoon) reduce the strength of the correlation, while the wet seasons (post-monsoon and monsoon) enhance the strength of the LST-NDBaI correlation.

The present study indicates that LST builds a stable and strong to moderate positive correlation with NDBaI in Raipur City, India throughout the study period. The result is comparable to the recently conducted other similar studies on the different urban agglomerations in the world. Essa et al (2012) have shown that NDBaI builds a positive correlation (0.39) with LST in the Greater Dublin region, Ireland. Chen and Zhang (2017) have shown the strong positive nature of the correlation coefficient of the LST-NDBaI relationship in a study performed in Kunming, China. A weak positive correlation between LST and NDBaI has been presented in London (0.086) and Baghdad (0.469) by Ali et al. (2017). This relationship was also positive (0.458) in Kolkata Metropolitan Area, India. The LST and NDBaI have built a weak negative correlation (-0.11) in Guangzhou, China. This correlation was weak positive (0.06) in Harare Metropolitan City, Zimbabwe. Sharma and Joshi (2016) have shown the moderate positive nature of LSI-NDBaI correlation in the National Capital Region of India. The present study shows that the average correlation coefficient between LST and NDBaI of all the four seasons from 1991-92 to 2018-19 is moderate positive (0.052), which can be considered as a very stable and authentic relationship between the two variables.

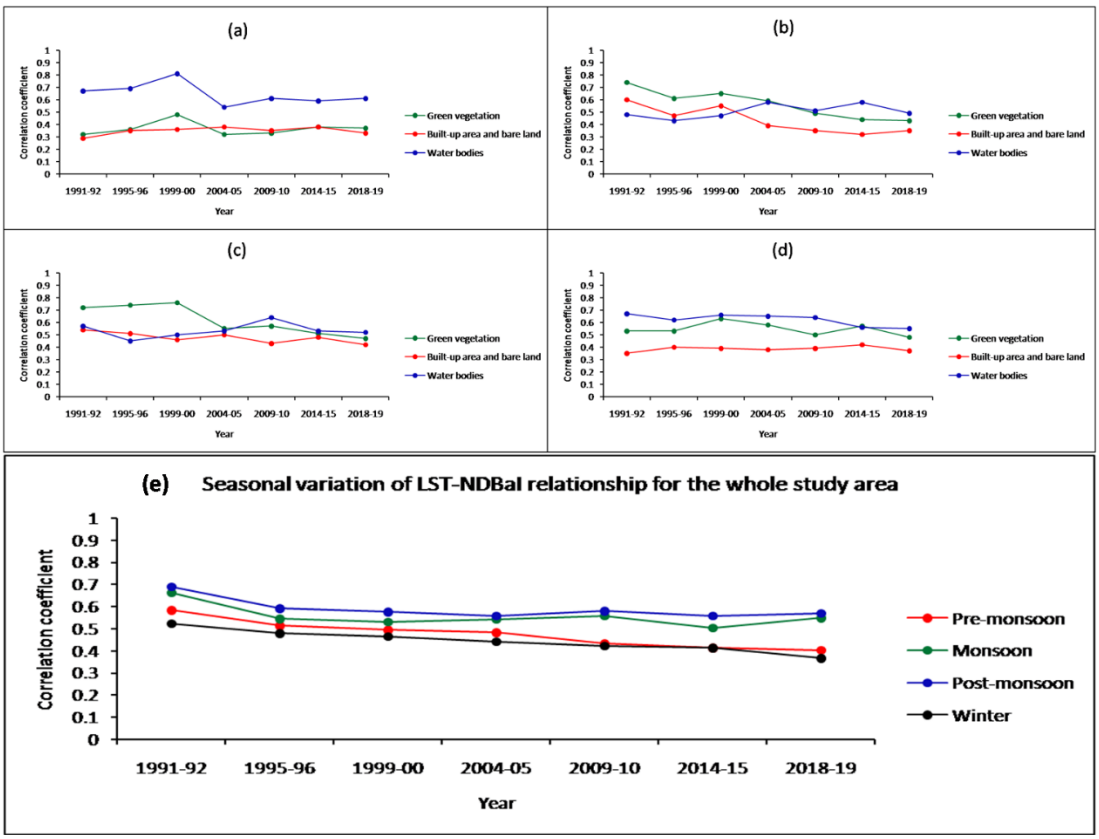

Figure 7. (a-d) Seasonal variation of the LST-NDBaI relationship on different types of LULC: (a) Pre-monsoon (b) Monsoon (c) Post-monsoon (d) Winter; (e) Seasonal variation of the LST-NDBaI relationship for the whole of the study area (significant at 0.05 level).

4. Conclusion

The present study analyzed the temporal and seasonal relationship of LST and NDBaI in Raipur City, India using sixty-five Landsat data sets of four different seasons (pre-monsoon, monsoon, post-monsoon, and winter) for different years. The main expectation was the relationship should be positive between LST and NDBaI across seasons. Moreover, another expectation was that the strength of the relationship should tend to be weaker with time. Another one is that the relationship should be stronger in comparatively wet season. The results support the expectations.

In general, the results show that LST is positively related to NDBaI, irrespective of any season. In the post-monsoon (0.59) and monsoon (0.56) seasons, the correlation is strongly positive, whereas it is found moderate positive in pre-monsoon (0.47) and winter (0.44). The LST-NDBaI relationship varies for specific LULC types. The water bodies reflect a strong positive correlation of LST-NDBaI in all the four seasons (0.65 in pre-monsoon, 0.51 in monsoon, 0.53 in post-monsoon, and 0.62 in winter). On green vegetation, this LST-NDBaI correlation is also strongly positive in monsoon (0.57), post-monsoon (0.62), and winter (0.55), whereas it is moderate positive in pre-monsoon (0.37) season. The built-up area and bare land build a moderate positive correlation of LST-NDBaI in all the four seasons (0.35 in pre-monsoon, 0.43 in monsoon, 0.48 in post-monsoon, and 0.39 in winter).

Among the four seasons, the post-monsoon season builds the best LST-NDBaI correlation for all LULC types, whereas the pre-monsoon season has the least correlation. Among the various LULC categories, the water bodies present the best positive LST-NDBaI correlation (0.65 in pre-monsoon, 0.51 in monsoon, 0.53 in post-monsoon, and 0.62 in winter), irrespective to any season. Green vegetation shows strong positive (0.57 in monsoon, 0.62 in post-monsoon, and 0.55 in winter) to moderate positive (0.37 in pre-monsoon) correlation between LST and NDBaI. On the other hand, the bare land and built-up area present a moderate positive correlation (0.35 in pre-monsoon, 0.43 in monsoon, 0.48 in post-monsoon, and 0.39 in winter). Among the four seasons, the post-monsoon season builds the best LST-NDBaI correlation for all LULC types, whereas the pre-monsoon season has the least correlation. The high ratio of green plants and water surface can enhance the ecological health. Thus, this research work can be beneficial for the environmental planners.

5. Acknowledgment

The author is indebted to the United States Geological Survey (USGS).

6. Disclosure statement

No potential conflict of interest was reported by the author.

References

Ahmed B, Kamruzzaman M, Zhu X, Rahman MS, Choi K. Simulating Land Cover Changes and Their Impacts on Land Surface Temperature in Dhaka, Bangladesh. *Remote Sens.* 2013;5(11):5969-5998. https://doi.org/10.3390/rs5115969

Alexander C. Normalised difference spectral indices and urban land cover as indicators of land surface temperature (LST). *Int. J. Appl. Earth Obs. Geoinf.* 2020;86:102013. https://doi.org/10.1016/j.jag.2019.102013

Alibakhshi Z, Ahmadi M, Farajzadeh Asl M. Modeling Biophysical Variables and Land Surface Temperature Using the GWR Model: Case Study—Tehran and Its Satellite Cities. *J. Indian Soc. Remote Sens.* 2020;48:59–70. https://doi.org/10.1007/s12524-019-01062-x

Ali JM, Marsh SH, Smith MJ. A comparison between London and Baghdad surface urban heat islands and possible engineering mitigation solutions. *Sustain. Cities Soc.* 2017;29:159-168. https://doi.org/10.1016/j.scs.2016.12.010

As-syakur AR, Adnyana IWS, Arthana IW, Nuarsa IW. Enhanced Built-Up and Bareness Index (EBBI) for Mapping Built-Up and Bare Land in an Urban Area. *Remote Sens.* 2012;4(10):2957-2970. https://doi.org/10.3390/rs4102957

Barsi J, Schott J, Hook S, Raqueno N, Markham B, Radocinski R. Landsat-8 thermal infrared sensor (TIRS) vicarious radiometric calibration. *Remote Sens.* 2014;6(11):11607-11626.

Carlson TN, Ripley DA. On the Relation between NDVI, Fractional Vegetation Cover, and Leaf Area Index. *Remote Sens. Environ.* 1997;62:241-252. https://doi.org/10.1016/S0034-4257(97)00104-1

Chen XL, Zhao HM, Li PX, Yi ZY. Remote sensing image-based analysis of the relationship between urban heat island and land use/cover changes. *Remote Sens. Environ.* 2006;104(2):133–146. https://doi.org/10.1016/j.rse.2005.11.016

Chen X, Zhang Y. Impacts of urban surface characteristics on spatiotemporal pattern of land surface temperature in Kunming of China. *Sustain. Cities Soc.* 2017;32:87-99. https://doi.org/10.1016/j.scs.2017.03.013

Essa W, Verbeiren B, Van der Kwast J, Van de Voorde T, Batelaan O. Evaluation of the DisTrad thermal sharpening methodology for urban areas. *Int. J. Appl. Earth Obs. Geoinf.* 2012;19:163-172. https://doi.org/10.1016/j.jag.2012.05.010

Guha S, Govil H, Diwan P. Analytical study of seasonal variability in land surface temperature with normalized difference vegetation index, normalized difference water index, normalized difference built-up index, and normalized multiband drought index. *J. Appl. Remote Sens.* 2019;13(2): 024518. https://doi.org/1010.1117/1.JRS.13.024518

Guha S, Govil H, Gill N, Dey A. Analytical study on the relationship between land surface temperature and land use/land cover indices. *Ann. GIS.* 2020;26(2): 201-216. https://doi.org/10.1080/19475683.2020.1754291

Guha S, Govil H, Mukherjee S. Dynamic analysis and ecological evaluation of urban heat islands in Raipur city, India. *J. Appl. Remote Sens.* 2017;11(3): 036020. https://doi:10.1117/1.JRS.11.036020

Guo G, Wu Z, Chen Y. Estimation of subpixel land surface temperature using Landsat TM imagery: A case examination over a heterogeneous urban area. Third International Workshop on Earth Observation and Remote Sensing Applications

Hao X, Li W, Deng H. The oasis effect and summer temperature rise in arid regions-case study in Tarim Basin. *Sci. Rep.* 2016;6:35418. https://doi.org/10.1038/srep35418

Jain S, Sannigrahi S, Sen S, Bhatt S, Chakraborti S, Rahmat S. Urban heat island intensity and its mitigation strategies in the fast-growing urban area. *J. Urban Manage.* 2020;9(1):54-66. https://doi.org/10.1016/j.jum.2019.09.004

Li J. Estimating land surface temperature from Landsat-5 TM. Remote Sens. Technol. Appl. 2006;21:322-326.

Li ZN, Duan SB, Tang BH, Wu H, Ren HG, Yan GJ. Review of methods for land surface temperature derived from thermal infrared remotely sensed data. *J. Remote Sens.* 2016;20:899–920.

Macarof P, Bîrlica IC, Stătescu F. Investigating the relationship between land surface temperature and urban indices using landsat-8: a case study of Iaşi. *Lucrările Seminarului Geografic Dimitrie Cantemir* 2017;45:81-88. https://doi.org/10.15551/lsgdc.v45i0.07

Mushore TD, Odindi J, Dube T, Mutanga O. Prediction of future urban surface temperatures using medium resolution satellite data in Harare metropolitan city, Zimbabwe. *Build. Environ.* 2017;122:397-410. https://doi.org/10.1016/j.buildenv.2017.06.033

Nimish G, Bharath HA, Lalitha A. Exploring temperature indices by deriving relationship between land surface temperature and urban landscape. *Remote Sens. Appl. Soc. Environ.* 2020;18:100299. https://doi.org/10.1016/j.rsase.2020.100299

Qin Z, Karnieli A, Barliner P. A Mono-Window Algorithm for Retrieving Land Surface Temperature from Landsat TM Data and Its Application to the Israel-Egypt Border Region. *Int. J. Remote Sens.* 2001;22(18):3719-3746. https://doi:10.1080/01431160010006971

Sharma R, Joshi PK. Mapping environmental impacts of rapid urbanization in the National Capital Region of India using remote sensing inputs. *Urban Clim.* 2016;15:70-82. https://doi.org/10.1016/j.uclim.2016.01.004

Yuan X, Wang W, Cui J, Meng F, Kurban A, De Maeyer. Vegetation changes and land surface feedbacks drive shifts in local temperatures over Central Asia. *Sci. Rep.* 2017;(1):3287. https://doi.org/10.1038/s41598-017-03432-2

Sekertekin A, Bonafoni S. Land surface temperature retrieval from landsat 5, 7, and 8 over rural areas: assessment of different retrieval algorithms and emissivity models and toolbox implementation. *Remote Sens.* 2020;12(2):294. https://doi.org/10.3390/rs12020294

Sharma R, Ghosh A, Joshi PK. Mapping environmental impacts of rapid urbanization in the National Capital Region of India using remote sensing inputs. *Geocarto Int.* 2013;28(5):420-438. https://doi.org/10.1080/10106049.2012.715208

(EORSA), Changsha, 2014. p. 304-308. https://doi.org/10.1109/EORSA.2014.6927900

Sobrino JA, Raissouni N, Li Z. A comparative study of land surface emissivity retrieval from NOAA data. *Remote Sens. Environ.* 2001;75(2):256–266. https://doi.org/10.1016/S0034-4257(00)00171-1

Sobrino JA, Jimenez-Munoz JC, Paolini L. Land surface temperature retrieval from Landsat TM5. *Remote Sens. Environ.* 2004;9:434–440. https://doi:10.1016/j.rse.2004.02.003

Sun Q, Tan J, Xu Y. An ERDAS image processing method for retrieving LST and describing urban heat evolution: A case study in the Pearl River Delta Region in South China. *Environ. Earth Sci.* 2010;59:1047-1055.

Tomlinson CJ, Chapman L, Trones JE, Baker C. Remote sensing land surface temperature for meteorology and climatology: a review. *Meteorol. Appl.* 2011;118:296–306. https://doi.org/10.1002/met.287

Wang J, Qingming Z, Guo H, Jin Z. Characterizing the Spatial Dynamics of Land Surface temperature–impervious Surface Fraction Relationship. *Int. J. Appl. Earth Obs. Geoinf.* 2016;45:55–65.

Weng QH, Lu DS, Schubring J. Estimation of Land Surface Temperature–Vegetation Abundance Relationship for Urban Heat Island Studies. *Remote Sens. Environ.* 2004;89:467-483. https://doi:10.1016/j.rse.2003.11.005

Weng Q, Quattrochi DA. Thermal remote sensing of urban areas: An introduction to the special issue. *Remote Sens. Environ.* 2006;104(2):119-122. https://doi.org/10.1016/j.rse.2006.05.002

Wukelic GE, Gibbons DE, Martucci LM, Foote HP. Radiometric calibration of Landsat Thematic Mapper thermal band. *Remote Sens. Environ.* 1989;28:339–347. https://doi.org/10.1016/0034-4257(89)90125-9

Yang J, Que J. The empirical expressions of the relation between precipitable water and ground water vapor pressure for some areas in China. *Sci. Atmos. Sin.* 1996;20:620-626.

Zanter K. Landsat 8 (L8) Data Users Handbook; EROS: Sioux Falls, SD, USA. 2019.

Zhao HM, Chen XL. Use of normalized difference bareness index in quickly mapping bare areas from TM/ETM+. Geoscience and Remote Sensing Symposium. 2005;3(25–29):p.1666−1668. https://doi.org/10.1109/IGARSS.2005.1526319